Autophagy 10:7, 1285–1300; July 2014; © 2014 Landes Bioscience

Activation of the MAPK11/12/13/14 (p38 MAPK) pathway regulates the transcription of autophagy genes in response to oxidative stress induced by a novel copper complex in HeLa cells

Wu Zhong,[1,†] Haichuan Zhu,[1,2,†] Fugeng Sheng,[3] Yonglu Tian,[4] Jun Zhou,[1] Yingyu Chen,[5] Song Li,[1,*] and Jian Lin[2,*]

[1]Laboratory of Computer-Aided Drug Design and Discovery; Beijing Institute of Pharmacology and Toxicology; Beijing, China; [2]Synthetic and Functional Biomolecules Center; College of Chemistry and Molecular Engineering; Peking University; Beijing, China; [3]Department of Radiology; Affiliated Hospital of the Academy of Military Medical Science; Beijing, China; [4]Laboratory Animal Centre; Peking University; Beijing, China; [5]Centre for Human Disease Genomics; Peking University; Beijing, China

[†]These authors contributed equally to this work.

Keywords: cHYF127c/Cu, MAPK11, MAPK12, MAPK13, MAPK14, autophagy, copper, oxidative stress, p38 mitogen-activated protein kinase, transcription

Abbreviations: ATG, autophagy-related; CASP3, caspase 3, apoptosis-related cysteine peptidase; CQ, chloroquine; Cis, cisplatin; Cu, copper; HYF127c, di-2-pyridyl Ketone 4-allyl-3-Selenosemicarbazide; LC3, microtubule-associated protein 1 light chain 3; MAPK, mitogen-activated protein kinase; MAPK8/JNK1, mitogen-activated protein kinase 8; MAPK9/JNK2, mitogen-activated protein kinase 9; MAPK10/JNK3, mitogen-activated protein kinase 10; MAPK11/p38Beta, mitogen-activated protein kinase 11; MAPK12/p38gamma, mitogen-activated protein kinase 12; MAPK13/p38delta, mitogen-activated protein kinase 13; MAPK14/p38alpha, mitogen-activated protein kinase 14; MTT, 3-(4,5)-dimethylthiahiazo (-z-y1)-3,5-di-phenytetrazoliumromide; NAC, N-acetyl-L-cysteine; NEC-1, necrostatin-1; SB203580, 4-(4-fluorophenyl)-2-(4-methylsulfinylphenyl)-5-(4-pyridyl)-1H-imidazole; Rapa, rapamycin; SP600125, 1,9-pyrazoloanthrone anthrapyrazolone; 3MA, 3-methyladenine; Z-VAD-fmk, N-benzyloxycarbonyl-Val-Ala-Asp(O-Me) fluoromethyl ketone

Transition metal copper (Cu) can exist in oxidized or reduced states in cells, leading to cytotoxicity in cancer cells through oxidative stress. Recently, copper complexes are emerging as a new class of anticancer compounds. Here, we report that a novel anticancer copper complex (HYF127c/Cu) induces oxidative stress-dependent cell death in cancer cells. Further, transcriptional analysis revealed that oxidative stress elicits broad transcriptional changes of genes, in which autophagy-related genes are significantly changed in HYF127c/Cu-treated cells. Consistently, autophagy was induced in HYF127c/Cu-treated cells and inhibitors of autophagy promoted cell death induced by HYF127c/Cu. Further analysis identified that the MAPK11/12/13/14 (formerly known as p38 MAPK) pathway was also activated in HYF127c/Cu-treated cells. Meanwhile, the MAPK11/12/13/14 inhibitor SB203580 downregulated autophagy by inhibiting the transcription of the autophagy genes *MAP1LC3B, BAG3*, and *HSPA1A*, and promoted HYF127c/Cu-induced cell death. These data suggest that copper-induced oxidative stress will induce protective autophagy through transcriptional regulation of autophagy genes by activation of the MAPK11/12/13/14 pathway in HeLa cells.

Introduction

Metal (e.g., platinum, gold, and copper) complexes have shown an enormous potential for use in cancer chemotherapy.[1-7] For example, cisplatin and its derivatives (carboplatin and oxaliplatin) are widely applied in chemotherapeutics against a wide variety of cancers.[8] Recently copper complexes have attracted more attention.[9-11] The disulfiram (DSF)-copper complex efficiently induces apoptosis in breast cancer cells.[12] The di-2-pyridylketone-4,4,-dimethyl-3-thiosemicarbazone (Dp44mT)-copper complex disrupts lysosomes and induces apoptosis in human neuroepithelioma SK-N-MC cells.[13] Pyrazole-pyridine copper complexes induce paraptotic cell death in different cancer cells.[14] In addition, copper complexes can also efficiently inhibit proteasome activity in cancer cells.[11] These results imply that copper complexes could target multiple pathways in cancer cells.

*Correspondence to: Jian Lin; Email: linjian@pku.edu.cn; Song Li; Email: lis@bmi.ac.cn
Submitted: 07/09/2013; Revised: 03/27/2014; Accepted: 04/04/2014; Published Online: 05/12/2014
http://dx.doi.org/10.4161/auto.28789

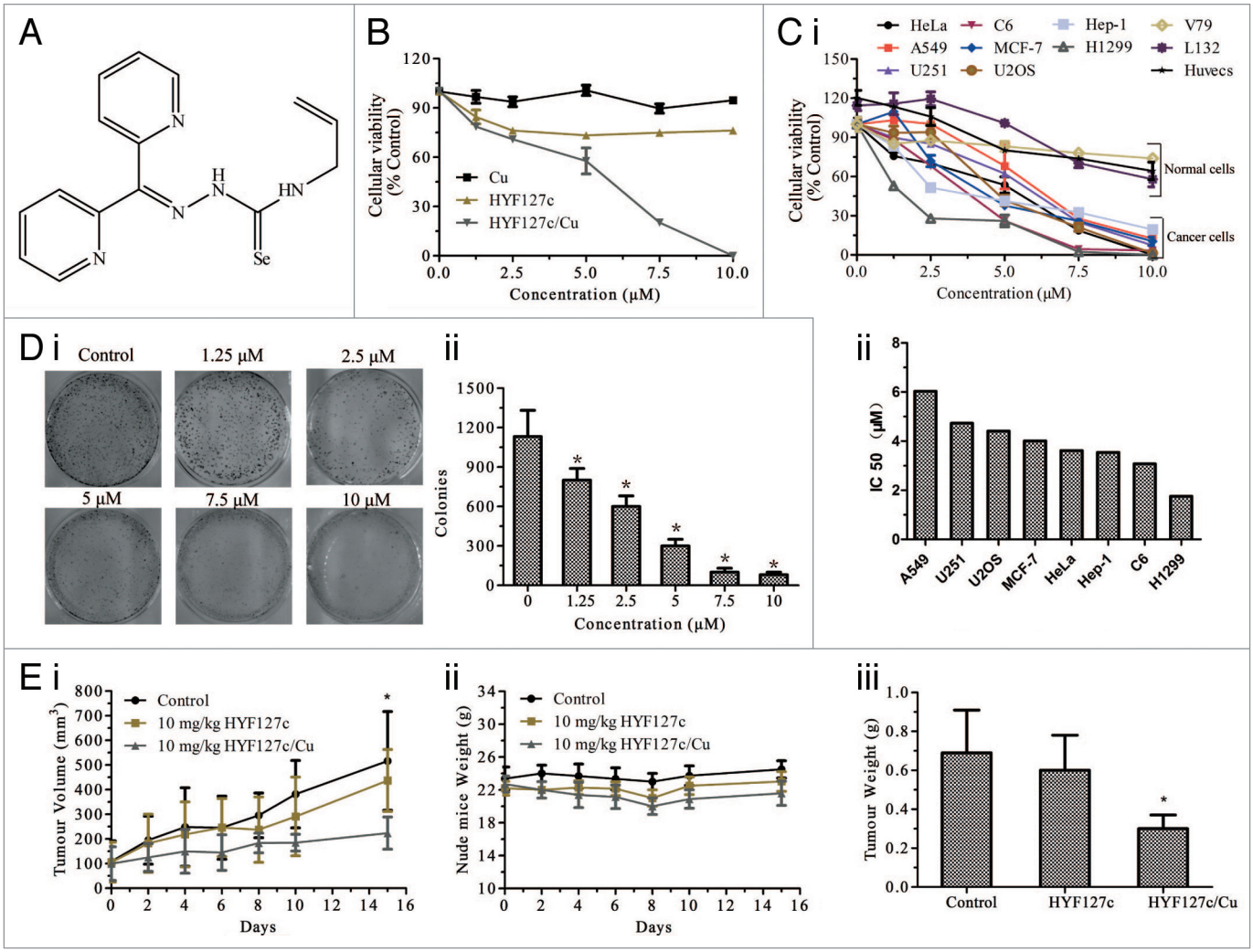

Figure 1. HYF127c/Cu induces cancer cell death and inhibits tumor growth in vivo. (**A**) The molecular structure of HYF127c (4-allyl-3-selenosemicarbazide). (**B**) Effect of HYF127c/Cu on the survival of HeLa cells. HeLa cells were exposed for 12 h to different concentrations of HYF127c, $CuCl_2$, or HYF127c/Cu. Cell viability was determined by MTT assay and expressed as the percentage of survival cells. (**C**) Effect of HYF127c/Cu on the survival of cancer cells and normal cells. (i) Cellular viability of cancer cells and normal cells treated with different concentrations of HYF127c/Cu for 12 h. Each sample was measured in triplicate. (ii) IC_{50} of HYF127c/Cu in cancer cells. (**D**) Effect of HYF127c/Cu on the formation of colonies in HeLa cells. (i) Representative images of colonies treated with different concentrations of HYF127c/Cu. (ii) Statistics of the formation of colonies in HeLa cells treated with different concentrations of HYF127c/Cu (n = 3, *$P < 0.05$). (**E**) (i) Effect of HYF127c/Cu on tumor volume in human tumor xenografts. (ii) Effect of HYF127c/Cu on the weights of human tumor xenografts. (iii) Effect of HYF127c/Cu on tumor weight in human tumor xenografts (n = 8, *$P < 0.05$).

Autophagy is a degradation process that delivers cytoplasmic materials to lysosomes through autophagosomes in cells.[15] Although autophagy is associated with cell death in copper complex-treated cells, the role of copper complex-induced autophagy in cell death is not well defined.[16-22] The copper complex 2-pyridinecarbaldehyde *N*, *N*-bis (2-pyridinylmethyl) thiosemicarbazone (NSC 689534) induces autophagy through oxidative stress.[20] Cas III-ia induces autophagy and apoptosis in glioma cells through oxidative stress and activation of the MAPK8/9/10 (formerly known as JNK) pathway.[18] These results suggest that activation of autophagy may be a common phenomenon in cells treated with copper complexes.

Here, we report a novel anticancer copper complex (HYF127c/Cu) induces oxidative stress-dependent cell death in cancer cells. Our results showed that HYF127c/Cu induces protective autophagy in HeLa cells. Transcriptional analysis by RNA-seq showed transcriptional changes of genes in autophagy. Further analysis revealed that the MAPK11/12/13/14 pathway participates in the transcriptional regulation of autophagy-related genes, which contributes to the protection of HYF127c/Cu-induced cell death.

Results

A novel copper complex (HYF127c/Cu) efficiently induces oxidative stress-mediated cell death in cancer cells

During the search of selenium compounds that inhibit the proliferation of cancer cells, we discovered that a copper complex HYF127c/Cu, which is the HYF127c (di-2-pyridyl

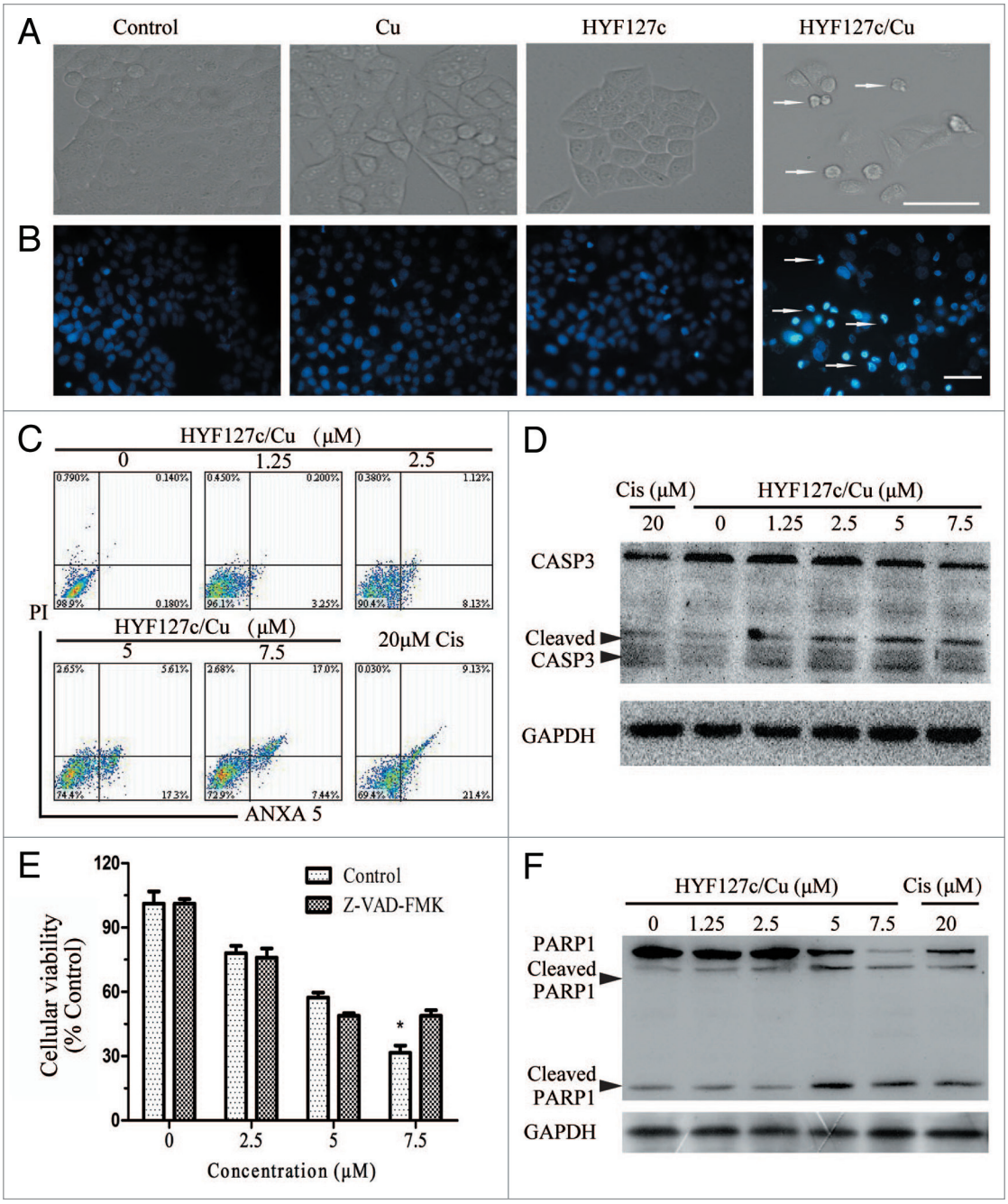

Figure 2. HYF127c/Cu induces apoptosis in HeLa cells. (**A**) Morphology changes in HeLa cells treated with HYF127c/Cu. Scale bar: 50 μm. (**B**) Nuclear changes in HeLa cells treated with HYF127c/Cu (arrows indicate the condensation of chromatins). Scale bar: 50 μm. (**C**) ANXA5-propidium iodide (PI) staining of HeLa cells treated with different concentrations of HYF127c/Cu. (**D**) Western blot results of CASP3 in HeLa cells treated with different concentrations of HYF127c/Cu. (**E**) Effect of z-VAD-fmk on cellular viability of HeLa cells treated with of HYF127c/Cu (n = 3, **P* < 0.05). (**F**) Western blot results of PARP1 in HeLa cells treated with different concentrations of HYF127c/Cu.

ketone 4-allyl-3-selenosemicarbazide, **Fig. 1A**) complex with copper, efficiently reduced viability in HeLa cervical cancer cells in a dose-dependent manner (**Fig. 1B and C**). Consistently, HYF127c/Cu treatment inhibited the proliferation of HeLa cells (data not shown). Furthermore, we investigated the effect of HYF127c/Cu on the viability of various cancer cells and normal cells by MTT. HYF127c/Cu efficiently suppressed the viability of other cancer cells (including human lung adenocarcinoma epithelial A549 cells, human non-small cell lung carcinoma H1299 cells, human glioma U251 cells, rat glioma C6 cells, human breast cancer MCF-7 cells and human osteosarcoma U2os cells) in a dose-dependent manner (**Fig. 1C, i**). IC_{50} results showed that H1299 cells were much more sensitive to HYF127c/Cu, while others such as HeLa and A549 cells were more resistant (**Fig. 1C, ii**). Importantly, HYF127c/Cu had much less cytotoxicity on normal cells (Chinese hamster lung fibroblast

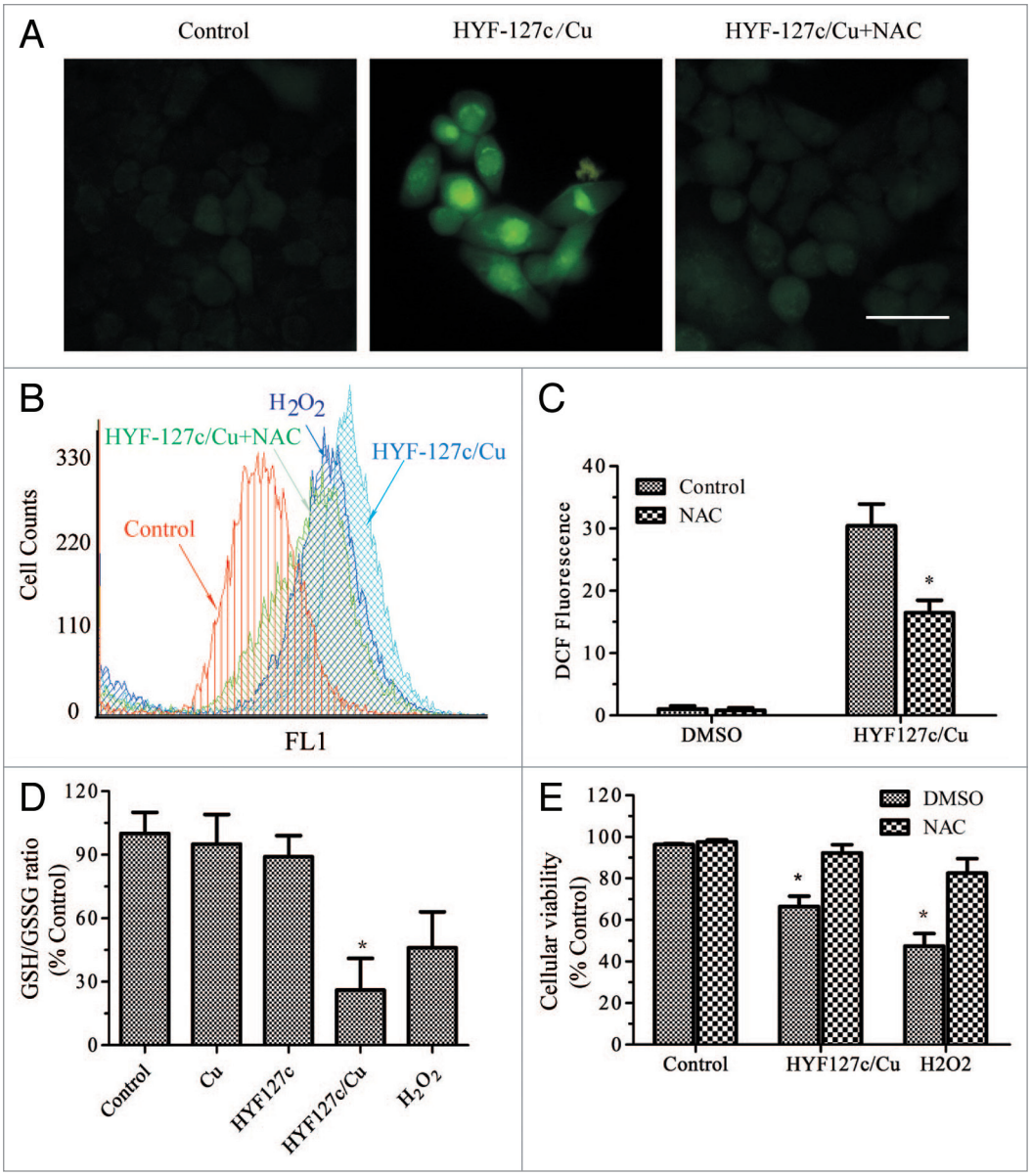

Figure 3. HYF127c/Cu induces cell death through oxidative stress. (**A**) Cells were treated with DMSO, 5 μM HYF127c/Cu or an additional 5 mM NAC treatment for 12 h. After incubation with 10 μM H_2DCFDA, cells were washed and examined by fluorescence microscopy. Scale bar: 20 μm. (**B**) Cells were treated with the indicated compounds for 12 h. After incubation with 10 μM H2DCFDA, cells were washed and examined by flow cytometry. (**C**) Average fluorescence intensity from DCF. (**D**) Cells were treated with DMSO, 5 μM Cu, 5 μM HYF127c, 5 μM HYF127c/Cu, or 5 μM H_2O_2 for 12 h. GSH and GSSG were measured with a microplate reader. The relative ratio is shown as indicated (n = 3, **P* < 0.05). (**E**) The relative ratio of cellular viability in cells treated with combinational compounds as indicated (n = 3, **P* < 0.05).

V79 cells, human embryonic lung L132 cells, and human umbilical vein endothelial Huvecs cells) (**Fig. 1C**, **i**). These results indicated that HYF127c/Cu could have the potential to selectively kill cancer cells. To further confirm that HYF127c/Cu inhibited the growth of cancer cells, we investigated whether it could efficiently inhibit the formation of colonies. The result showed that HYF127c/Cu treatment efficiently inhibited the formation of colonies of HeLa cells in a dose-dependent manner (**Fig. 1D**). Thus, HYF127c/Cu can efficiently induce cytotoxicity in cancer cells.

Then, we investigated whether HYF127c/Cu could inhibit tumor growth in human tumor xenografts. HeLa cells were implanted subcutaneously in female nude mice. When tumor size reached about 100 mm^3 the mice were randomly grouped and treated daily with either vehicle control, 10 mg/kg HYF127c or 10 mg/kg HYF127c/Cu. During the treatment, tumor volumes were measured as indicated (**Fig. 1E**, **i**). The weight of the mice was not perceptibly changed (**Fig. 1E**, **ii**). In the last step, the mice were sacrificed and the tumors were removed for weighing. HYF127c/Cu significantly inhibited tumor growth by 56% ($P < 0.01$) compared with the control (**Fig. 1E**, **iii**). In addition, the histological results from kidney, myocardium, and liver in nude mice showed that these organs were not visibly damaged by HYF127c/Cu (**Fig. S1**), suggesting the safety of HYF127c/Cu at this dosage. Therefore, HYF127c/Cu efficiently inhibits tumor growth in vivo.

Then we investigated the type of cell death in HYF127c/Cu-treated cancer cells. HYF127c/Cu treatment induced perceptible morphology changes in HeLa cells. Cells were detached from the surface with cell shrinkage (**Fig. 2A**). It is different from paraptotic cell death, which exhibits significant vacuolation in the cytoplasm. In addition, condensation of chromatin was observed in HYF127c/Cu-treated cells (**Fig. 2B**). Early apoptotic cells were detected by fluorescein-labeled ANXA5/annexin A5 (**Fig. 2C**). Further, CASP3/caspase 3 and PARP1 were activated in HYF127c/Cu-treated cells (**Fig. 2D**

and F), and caspase inhibitor Z-VAD-fmk partially inhibited HYF127c/Cu-induced cell death (**Fig. 2E**). Meanwhile, the necrosis inhibitor Necrostatin-1 (NEC-1) did not inhibit HYF127c/Cu-induced cell death (**Fig. S2**). These results indicated that HYF127c/Cu induced apoptosis in HeLa cells.

Since copper complexes have been reported to induce cell death through induction of oxidative stress, we investigated whether HYF127c/Cu has a similar mechanism. The intracellular induction of oxidative stress in HeLa cells was assessed by the conversion of nonfluorescent H_2DCF to fluorescent DCF.[13,23] There was a significant increase of fluorescent DCF in HYF127c/Cu-treated HeLa cells after incubation for 12 h (**Fig. 3A–C**), while there were no evident fluorescent signal changes in cells treated with $CuCl_2$ or HYF127c alone (data not shown). In addition, the change of glutathione (GSH) into glutathione disulfide (GSSG) occurs when cells are subjected to oxidative stress, so the decrease of the ratio of GSH/GSSG (glutathione/glutathione disulfide) indicates oxidative stress in cells.[13] We measured the GSH/GSSG ratio in HYF127c/Cu-treated HeLa cells. The ratio of GSH/GSSG from HYF127c/Cu-treated HeLa cells was significantly reduced to about 25% of the control (**Fig. 3D**), implying that cellular GSH was obviously decreased in HYF127c/Cu-induced cell death. We next investigated whether the increase of oxidative stress contributed to HYF127c·Cu-induced cell death. HeLa cells were incubated with 5 μM HYF127c/Cu in the presence of 5 mM N-acety-L-cysteine (NAC), which is a widely used antioxidant.[24] NAC efficiently decreased oxidative stress induced by HYF127c/Cu (**Fig. 3A–C**), and significantly reduced HYF127c/Cu-induced cell death (**Fig. 3E**). These results suggested that HYF127c/Cu induced cell death through induction of oxidative stress

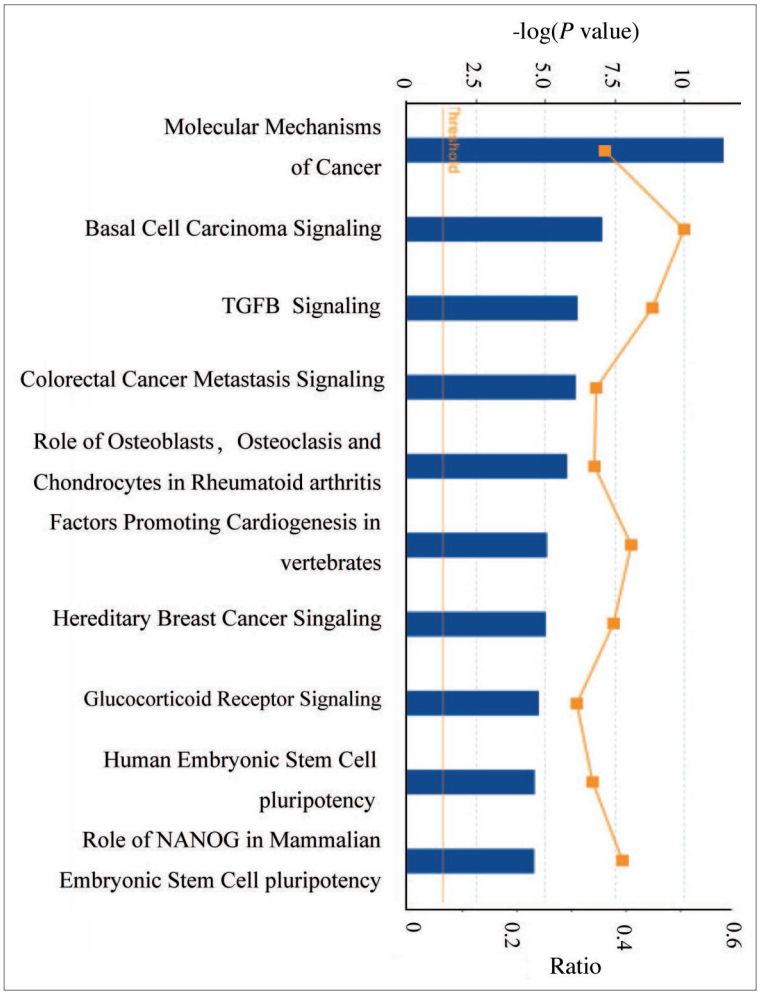

Figure 4. HYF127c/Cu induces broad transcriptional changes of genes in cancer-related pathways. Ingenuity software analysis (IPA) report of RNA-seq data arranged by signaling pathways in order of statistical significance. The top 10 ranked pathways are shown.

RNA-Seq analysis reveals that HYF127c/Cu induces broad transcriptional changes of genes involved in the molecular mechanism of cancer

RNA-seq is a powerful technique for the systemic analysis of transcriptome profiling in cells, which is increasingly being applied in biological, medical, and pharmaceutical research.[25] It can provide comprehensive and detailed information on complicated biological networks and pathways.[26] So it is an ideal tool to analyze transcriptional changes of cancer cells treated with anticancer compounds, although as of yet, little such work has been done.[27]

To identify genes differentially regulated in the process of HYF127c/Cu-induced cell death, HYF127c/Cu-treated cells and DMSO-treated (control) cells were processed for RNA-Seq. The sequencing data were compared and analyzed to identify genes participating in HYF127c/Cu-induced cell death (**Table S1**). Compared with the control, 1096 genes were upregulated (fold > 1, $P < 0.05$), while 4611 genes were downregulated (fold < –1, $P < 0.05$) in HYF127c/Cu-treated cells (**Table S1a and S1b**).

After that, we analyzed canonical signal networks and pathways by using the IPA software package (Ingenuity Systems Inc.). IPA can provide a global functional analysis of RNA-Seq data, which can be used to statistically rank various pathways in order of significance. Of more than 150 pathways ranked by IPA, the top ranked is the molecular mechanism of cancer pathway (**Fig. 4**). Consistent with IPA analysis results, a portion of genes in hallmarks of cancers are significantly changed in HYF127c/Cu-treated cells. (**Fig. 5**). These results indicate that HYF127c/Cu induces changes of multiple signal pathways in cancer cells.

Inhibition of autophagy promotes HYF127c/Cu-induced cell death

We were interested in finding a survival pathway that protected cancer cells from HYF127c/Cu-induced cell death. Many reports have shown that autophagy plays a protective role in cell death. However, IPA results of HYF127c/Cu-treated cells did not show changes in autophagy due to the absence of analysis of autophagy genes in the IPA database. So we directly analyzed transcriptional changes of autophagy-related genes in

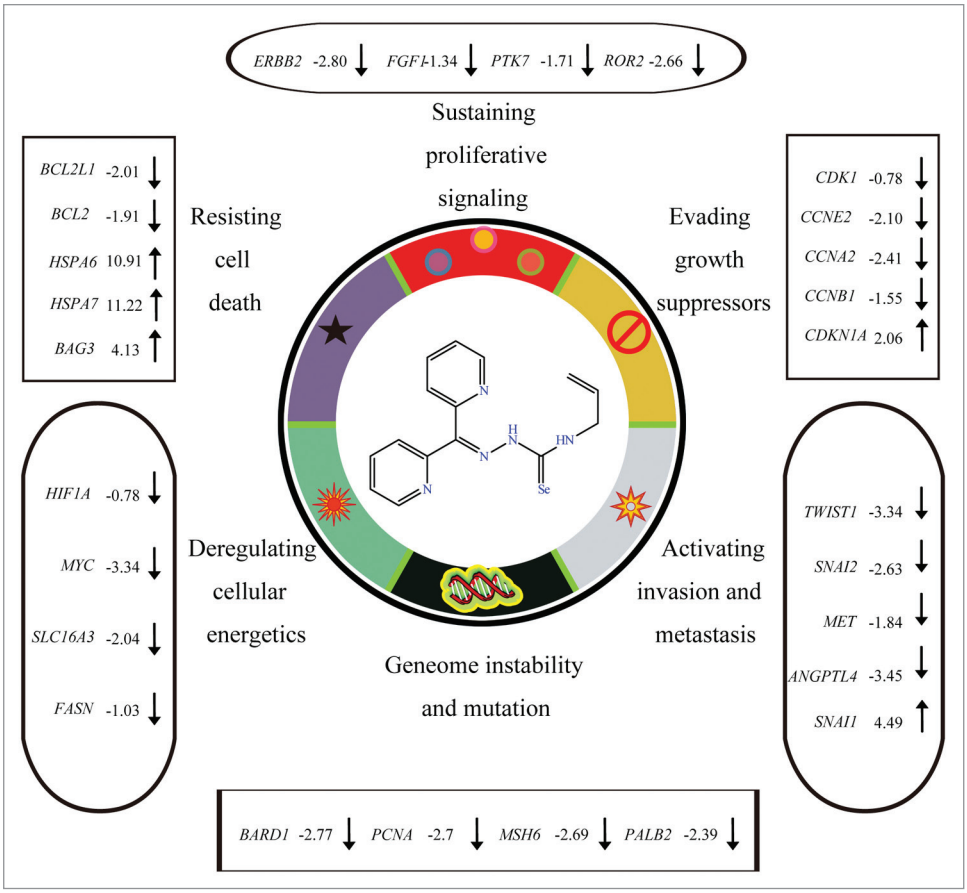

Figure 5. HYF127c/Cu induces significant changes of genes involved in hallmarks of cancers or enabling characteristics. Some of the genes significantly regulated by HYF127c/Cu are listed here.

HYF127c/Cu-treated cells from RNA-seq results. The results showed that genes in autophagy were changed in HYF127c/Cu-treated cells (**Table 1**). *DDIT3*,[28] *SESN2*,[29] *BAG3*,[30,31] and *HSPA1A/B*,[32] which can promote autophagy, were significantly upregulated in HYF127c/Cu-treated cells. Genes encoding LC3 proteins (*MAP1LC3B*, *MAP1LC3B2*, and *GABARAPL1*) were also upregulated. In addition, BCL2 family proteins (BCL2 and BCL2L1), which negatively regulate autophagy,[33-35] were significantly downregulated in HYF127c/Cu-treated cells.

Then we investigated whether autophagy was involved in the process of HYF127c/Cu-induced cell death. First, we examined acidic vesicular organelles in the cytoplasm by acridine orange (AO), which is frequently associated with autophagy.[36] There were a number of red fluorescent compartments in HYF127c/Cu-treated HeLa cells compared with the control cells (**Fig. 6A**). Then we examined vesicular accumulation of LC3 by assessing punctate EGFP-LC3 distribution in cells (**Fig. 6B**). A visible increase of punctate EGFP-LC3 was observed in HYF127c/Cu-treated cells (**Fig. 6B, i–iii**). Transmission electron microscopy (TEM) results showed the existence of double-membrane autophagosomes in HYF127c/Cu-treated HeLa cells (**Fig. 7A**) and the tumors from HYF127c/Cu-treated nude mouse (**Fig. S3**). In addition, western blot results showed that endogenous LC3-II was increased in HYF127c/Cu-treated cells (**Fig. 7B, i and iii**), and SQSTM1 was decreased by HYF127c/Cu in a dose-dependent manner (**Fig. 7B, ii and iv**). Further, there was evident colocalization of EGFP-LC3 puncta with LysoTracker Red-labeled lysosomes in HYF127c/Cu-treated cells (**Fig. 7C**), indicating that there were autolysosomes in HYF127c/Cu-treated cells. Taken together, these results indicate that HYF127c/Cu induces autophagy in HeLa cells.

Autophagy induced by anticancer compounds can either protect cancer cells from cell death or contribute to cancer cell death.[33,37-39] To investigate the role of HYF127c/Cu-induced autophagy in cell death, we examined HYF127c/Cu-induced cell death in *Atg7*$^{+/+}$ and *atg7*$^{-/-}$ mouse embryonic fibroblast (MEF) cells. *Atg7* is an essential gene for autophagy in cells.[36] HYF127c/Cu efficiently induced autophagy in *Atg7*$^{+/+}$ MEF cells, while it failed to induce autophagy in *atg7*$^{-/-}$ MEF cells as expected (**Fig. 8A and B**). HYF127c/Cu-induced cell death was increased in *atg7*$^{-/-}$ MEFs compared with that in *Atg7*$^{+/+}$ MEF cells, suggesting that knockout of *Atg7* increased HYF127c/Cu-induced cell death (**Fig. 8C**). Next, we investigated the effect of chloroquine (CQ) on the inhibition of lysosomal degradation of autophagosomes during HYF127c/Cu-induced cell death. An evident increase of EGFP-LC3 dots was observed in HeLa cells treated with CQ followed by HYF127c/Cu (**Fig. 8D**). Western blot analysis showed that endogenous LC3-II was increased in cells treated with both HYF127c/Cu and CQ (**Fig. 8E**). Meanwhile, the HYF127c/Cu-induced cell death rate was significantly increased by CQ (**Fig. 8F**) and 3-MA (**Fig. S4**). These results suggested that inhibition of autophagy increased cell death induced by HYF127c/Cu.

Meanwhile, we wondered whether autophagy had an effect on cellular ROS generated by HYF127c/Cu. HYF127c/Cu-induced cellular ROS was higher in *atg7*$^{-/-}$ MEFs compared with that in *Atg7*$^{+/+}$ MEF cells (**Fig. 8G, i and ii**). When HeLa cells were treated with both HYF127c/Cu and autophagy inhibitor 3-MA or CQ, cellular ROS was increased (**Fig. 8G, iii and iv**). However, when HeLa cells were treated with both HYF127c/Cu and the autophagy inducer rapamycin, cellular ROS was decreased compared with that in cells treated with HYF127c/Cu alone (**Fig. 8G, v**). These results suggested that autophagy could decrease HYF127c/Cu-induced cell death by decreasing cellular ROS.

Inhibition of the MAPK11/12/13/14 pathway downregulates HYF127c/Cu-induced autophagy by inhibiting the transcription of *BAG3*, *HSPA1A*, and *MAP1LC3B*

We tried to find a signal pathway that regulates HYF127c/Cu-induced autophagy and cell death by using the DAVID knowledge database (a functional annotation tool for gene functional classification, http://david.abcc.ncifcrf.gov/). We uploaded 652 genes that were significantly changed in HYF127c/Cu-treated cells (fold > 1 or fold < –1, $P < 0.01$ and FDR < 0.01, **Table S3**) to DAVID. The top 5 categories are sets of genes encoding phosphoproteins, nuclear proteins, metal binding proteins, transcription factors, and transcription regulation factors (**Fig. 7A**). So we hypothesized that pathways of phosphorylation would affect HYF127c·Cu-inducd autophagy and cell death. We analyzed phosphorylation signaling pathways by using IPA software and found that genes (fold > 1 or fold < –1, $P < 0.05$ and FDR < 0.05, **Table S4**) in several pathways such as the MAPK11/12/13/14 (p38 MAPK) pathway and the MAPK9/SAPK/JNK2 were significantly changed (–log(*P*) > threshold) in HYF127c/Cu-treated cells (**Fig. 9B**). Further, several genes (e.g., *JUN*, *FOS*, *EGR1*, and *MAFF*[40]) that have been reported to be transcriptionally activated by the MAPK11/12/13/14 pathway were also significantly upregulated in HYF127c/Cu-treated cells. Consistently, phosphorylation of both MAPK11/12/13/14 and its substrate MAPKAPK2/MK2 were increased in HYF127c/Cu-treated cells (**Fig. 9C**). To investigate whether activation of the MAPK11/12/13/14 pathway was related with HYF127c/Cu-induced autophagy and cell death, we treated HeLa cells with HYF127c/Cu and SB203580, a widely-used MAPK11/12/13/14 inhibitor.[41] HYF127c/Cu-induced cell death was enhanced by SB203580 (**Fig. 9D**). Meanwhile, SB203580 inhibited HYF127c/Cu-induced autophagy in HeLa cells (**Fig. 9E**). However, although SP600125 (a specific MAPK8/9/10 inhibitor[42]) could slightly reduce cellular viability in HYF127c/Cu-treated cells (**Fig. S5A**), it had no effect on HYF127c/Cu-induced autophagy (**Fig. S5B**). Further, SB203580 inhibited the increase of LC3-II and the decrease of SQSTM1 in HYF127c/Cu-treated cells (**Fig. 9F**). Finally, we investigated the effect of SB203580 on HYF127c/Cu-induced cell death in *Atg7*$^{+/+}$ and *atg7*$^{-/-}$ MEFs. SB203580 reduced cellular viability in HYF127c/Cu-treated *Atg7*$^{+/+}$ MEFs, while it had no obvious effect on cellular viability in HYF127c/Cu-treated *atg7*$^{-/-}$ MEFs (**Fig. 9G**). These results indicated that the MAPK11/12/13/14 pathway participated in the regulation of HYF127c/Cu-induced cell death.

Next we investigated whether the MAPK11/12/13/14 pathway regulated transcription of prosurvival genes in HYF127c/Cu-treated cell by real-time quantative PCR. We treated HeLa cells with the indicated compounds, then collected cells at different time points and extracted RNA for PCR. SB203580 significantly inhibited the transcription of *BAG3*, *MAP1LC3B*, and *HSPA1A*. Other genes (e.g., *ATG5*, *ATG7*, *BECN1*, *BCL2*, *SQSTM1*) were not significantly regulated by SB203580 (**Fig. 10**). Thus, MAPK14 regulates HYF127c/Cu-inducd cell death by increasing the transcription of the

Table 1. Transcriptional analysis of autophagy genes in HeLa cells treated with HYF127c·Cu

GeneID	Gene name	Fold changes	*P* value
HSPA1B	heat shock 70 kDa protein 1B	6.40	0.0004
HSPA1A	heat shock 70 kDa protein 1A	6.31	0.0004
SESN2	sestrin 2	4.67	0.0009
DDIT3	DNA-damage-inducible transcript 3	4.31	0.0000
BAG3	BCL2-associated athanogene 3	4.14	0.0003
ATG9B	autophagy-related 9B	3.28	0.0231
MAP1LC3B	microtubule-associated protein 1 light chain 3 β	2.92	0.0005
MAP1LC3B2	microtubule-associated protein 1 light chain 3 β 2	2.81	0.0004
GABARAPL1	GABA(A) receptor-associated protein like 1	1.37	0.0020
HSPB8	heat shock 22 kDa protein 8	1.31	0.0005
RB1CC1	RB1-inducible coiled-coil 1	1.05	0.0071
ATG4C	autophagy-related 4C, cysteine peptidase	–1.01	0.0094
ATG16L2	autophagy-related 16-like 2 (*S. cerevisiae*)	–1.12	0.0249
EIF4G1	eukaryotic translation initiation factor 4 gamma, 1	–1.24	0.0007
WIPI2	WD repeat domain, phosphoinositide interacting 2	–1.28	0.0008
ULK2	unc-51 like autophagy activating kinase 2	–1.29	0.0030
ATG2B	autophagy-related 2B	–1.57	0.0151
BAK1	BCL2-antagonist/killer 1	–1.62	0.0045
ATG16L1	autophagy-related 16-like 1 (*S. cerevisiae*)	–1.85	0.0015
RGS19	regulator of G-protein signaling 19	–1.89	0.0032
BCL2	B-cell CLL/lymphoma 2	–1.91	0.0003
ZKSCAN3	zinc finger with KRAB and SCAN domains 3	–1.92	0.0005
SLC33A1	solute carrier family 33 (acetyl-CoA transporter), member 1	–1.95	0.0019
BCL2L1	BCL2-like 1	–2.02	0.0007
TFEB	transcription factor EB	–2.09	0.0076
AMBRA1	autophagy/Beclin 1 regulator 1	–2.09	0.0051
VPS18	vacuolar protein sorting 18 homolog (*S. cerevisiae*)	–2.36	0.0034
SESN1	sestrin 1	–2.59	0.0034
TREX1	3 prime repair exonuclease 1	–2.69	0.0149
PIK3R4	phosphoinositide-3-kinase, regulatory subunit 4	–3.04	0.0024

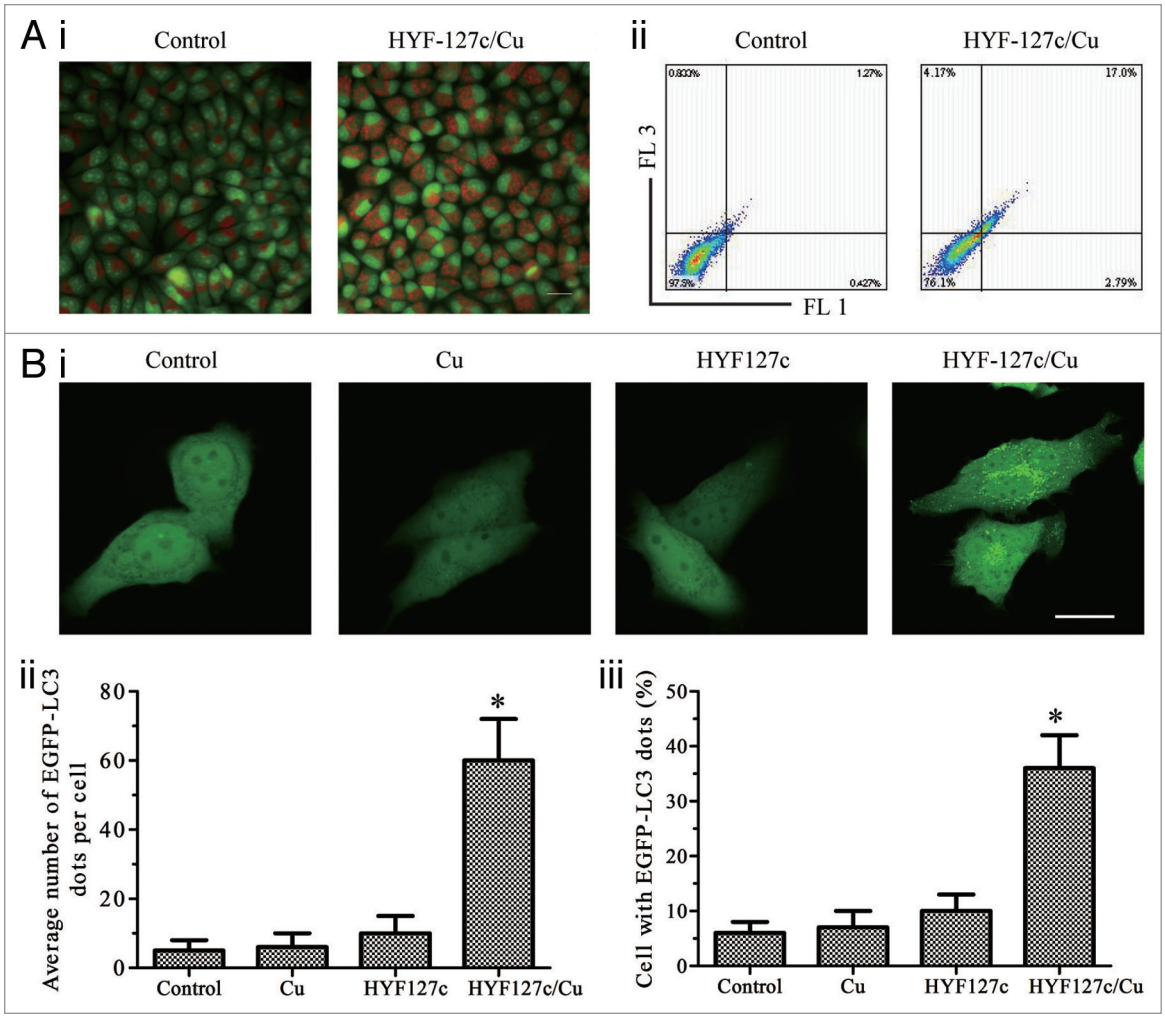

Figure 6. Fluorescent imaging results indicate that HYF127c/Cu induces autophagy in HeLa cells. (**A**) Accumulation of acidic vesicular organelles in HYF127c/Cu-treated HeLa cells. (i) Representative fluorescence images of cells treated with HYF127c/Cu or the control. In control cells, there was no red fluorescence from AO in the cytoplasm. However, there were many punctate red fluorescing compartments after treatment with 5 μM HYF127c/Cu for 12 h. Bar: 50 μm. (ii) Representative FACS results of cells treated with HYF127c/Cu or the control after AO staining. (**B**) Punctate distribution of EGFP-LC3 in HYF127c/Cu-treated cells. HeLa cells were transfected with EGFP-LC3 24 h before treatment with 5 μM HYF127c/Cu. Twelve h later, the punctate distribution of EGFP-LC3 was visualized and compared with the diffused distribution in control cells (i). Bar: 20 μm. The percentage of cells with evident accumulation of EGFP-LC3 dots (ii) and the average number of EGFP-LC3 dots in cells (iii) (n = 3, $^*P < 0.05$).

prosurvival autophagy genes *BAG3*, *HSPA1A,* and *MAP1LC3B*, which would contribute to resistance to cell death.

Discussion

Copper complexes are emerging novel metal complexes with anticancer activity.[1-7] It has been reported that copper complexes induce cancer cell death mainly through production of excess reactive oxygen species (ROS) and inhibition of proteasome activity.[9] Here, we reported that a novel compound HYF127c (4-allyl-3-Selenosemicarbazide) could form a copper complex and efficiently induce ROS-mediated cancer cell death. Furthermore, using RNA-Seq we discovered that a broad number of genes involved in cancer are transcriptional downregulated in HYF127c/Cu-treated HeLa cells (**Table S5**): First, many genes in the receptor tyrosine kinase family (e.g., *ERBB2/3, FGF2, PTK7, MET,* and *ROS1*) were all downregulated, which implies that HYF127c/Cu could negatively regulate pathways of receptor tyrosine kinases. Second, genes encoding cyclins (e.g., *CCNB1*, *CCND1*, *CCNE1*) and CDKs (e.g., *CDK1*, *CDK2*, *CDK4*, *CDK6*) were transcriptionally downregulated, which implies that HYF127c/Cu could inhibit the cell cycle process. Third, a portion of genes responsible for invasion and metastasis (e.g., *TWIST1*, *SNAI2/SLUG*, *MET*, and *ANGPTL4*) were significantly downregulated, which indicates that HYF127c/Cu could have an effect on the metastasis process. Fourth, critical genes for neoplastic lipogenesis (*ACLY*, *ACACA,* and *FASN*) were significantly downregulated, which indicates that HYF127c/Cu could negatively regulate lipid metabolism in cancer cells. Fifth, antiapoptotic genes such as *BCL2L1/Bcl-xL*, *BCL2*, *NAIP,* and

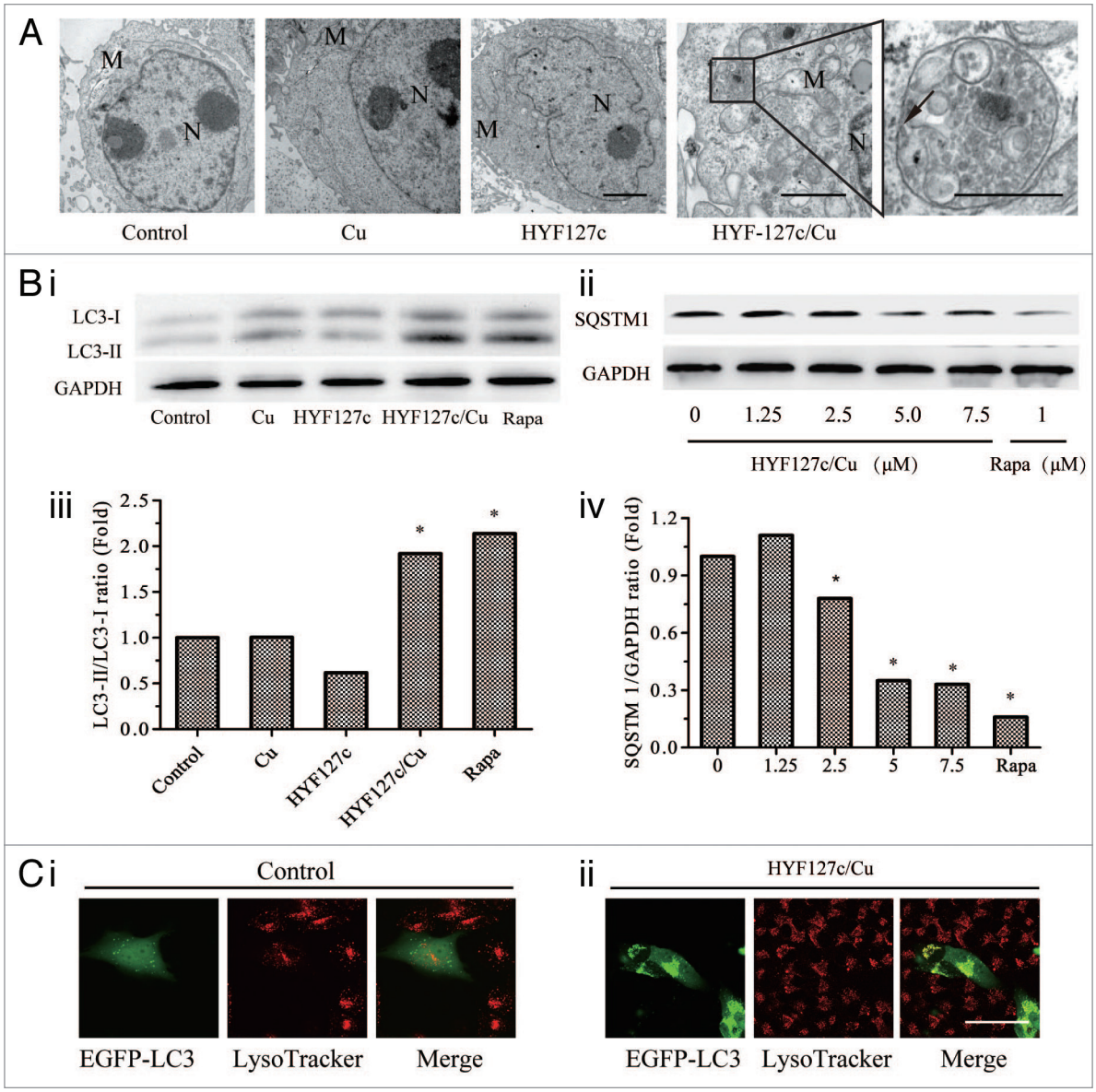

Figure 7. HYF127c/Cu induces autophagy in HeLa cells. (**A**) Electron microscopy images showing extensive cytoplasm vacuolization enclosed in a double membrane in HYF127c/Cu-treated HeLa cells. Electron microscopy image of an untreated cell is also shown for comparison. The double membrane of the autophagic vacuoles is indicated by a black arrow. N, nucleus; M, mitochondrion. Scale bar: 0.5 μm. (**B**) Conversion of LC3-I to LC3-II (i and iii) or degradation of SQSTM1 (ii and iv) in HYF127c/Cu-treated cells. HeLa cells were incubated with DMSO, 5 μM Cu, 5 μM HYF127c, 5 μM HYF127c/Cu or 1 μM rapamycin (control) and the amount of endogenous LC3-II proteins or SQSTM1 was analyzed by immunoblot. (**C**) The fluorescence images showing colocalization of lysosomes and autophagosomes in HYF127c/Cu-treated cells (ii) compared with the control (i). EGFP-LC3-transfected HeLa cells were stained with LysoTracker Red after 20 μM HYF127c/Cu treatment for 12 h. Bar: 20 μm.

BIRC3/c-IAP2 were significantly downregulated, suggesting that HYF127c·Cu could promote cancer cell death. In addition, genes encoding receptors of angiogenesis (e.g., *EGFR*) were downregulated, while *THBS1* (an angiogenesis inhibitor) was significantly upregulated, which suggests that HYF127c/Cu could have an inhibitory effect on angiogenesis. Thus, RNA-seq results indicate that HYF127c/Cu-induced oxidative stress could target multiple important pathways involved in cancer, and HYF127c/Cu could be a promising candidate for cancer therapy.

RNA-Seq also revealed that some autophagy genes (e.g., *MAP1LC3B*, *MAP1LC3B2,* and *ATG9B*) were upregulated in HYF127c/Cu-treated cells. Consistently, our experiments showed that HYF127c/Cu induced autophagy in HeLa cells. Although previous research reports that a copper complex induces autophagy in cell death,[43] little is known about the role of autophagy in copper complex-induced cell death. Autophagy can either protect cancer cells from cell death or promote cell death, which is becoming an important factor for cancer therapy.[44] Our results show that autophagy plays a protective role in HYF127c/Cu-induced cell death. The combination of copper complexes with autophagy inhibitors such as chloroquine (CQ) and 3-MA would significantly increase cancer cell death.

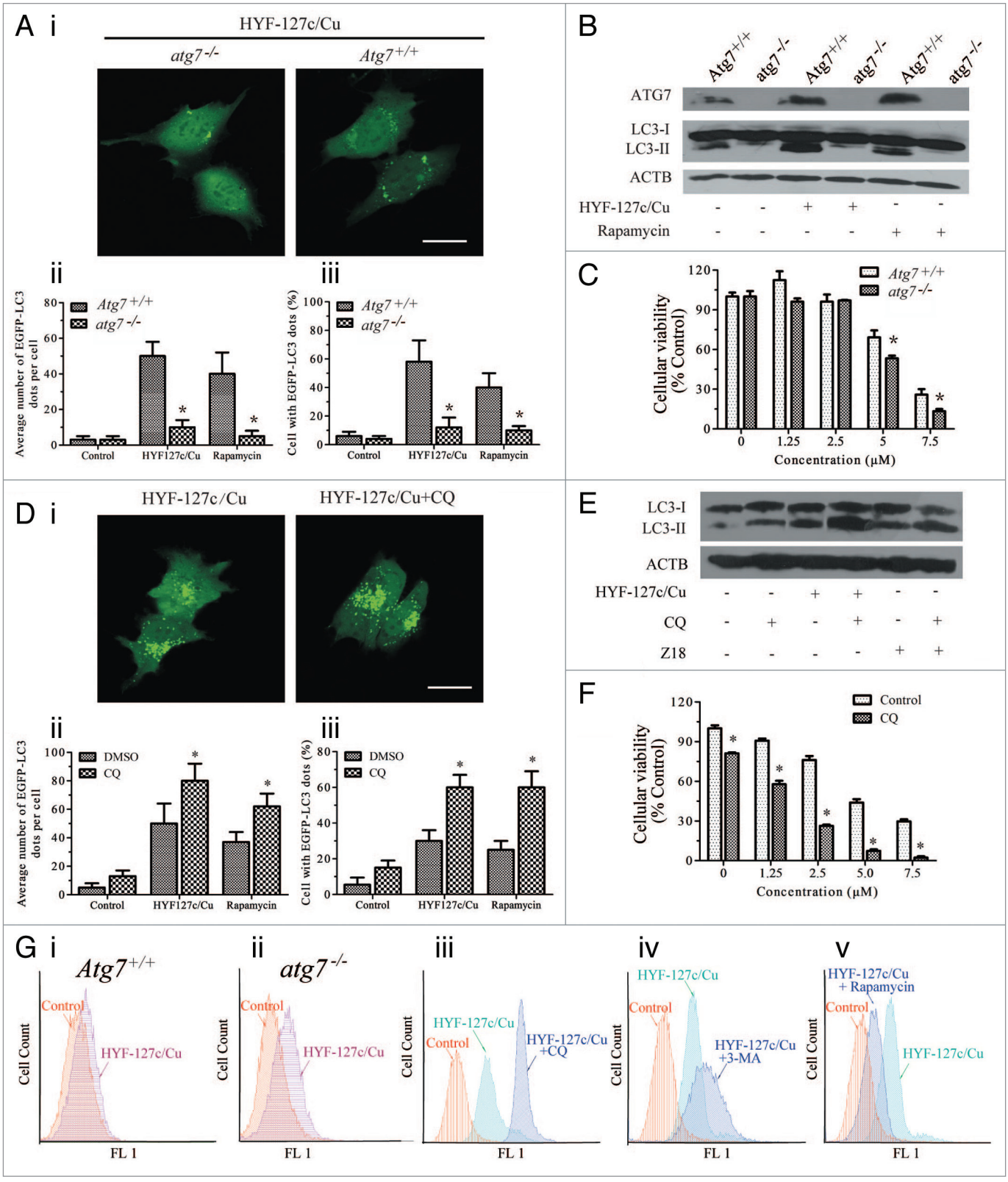

Figure 8. For figure legend, see page 1295.

Figure 8 (See opposite page). Inhibition of autophagy promotes HYF127c/Cu-induced cell death. (**A**) Effect of *Atg7* on HYF127c/Cu induced autophagy. Decreased punctate distribution of EGFP-LC3 in *atg7*$^{-/-}$ MEF cells treated with HYF127c/Cu (i). Bar: 20 μm. The average number of EGFP-LC3 dots in cells (ii) and the percentage of cells with evident accumulation of EGFP-LC3 dots (iii). (n = 3, *P < 0.05). (**B**) Effect of *Atg7* on the conversion of LC3-I to LC3-II in HYF127c/Cu-treated cells. Western blots showed that ATG7 deficiency inhibits LC3-I conversion. (**C**) The effect of *Atg7* deficiency on cellular viability, (n = 3, *P < 0.05). (**D**) CQ inhibits HYF127c/Cu-induced autophagy. (i) Increased punctate distribution of EGFP-LC3 in cells treated with HYF127c/Cu and CQ. Bar: 20 μm. (ii) The percentage of cells with evident accumulation of EGFP-LC3 dots. (iii) The average number of EGFP-LC3 dots in cells. (n = 3, *P < 0.05). (**E**) Conversion of LC3-I to LC3-II in cells treated with HYF127c/Cu and CQ or HYF127c/Cu alone. Z18, a previously reported autophagy inducer,[39] was used as a control. (**F**) The effect of the combination of CQ and HYF127c/Cu on cellular viability of HeLa cells. (n = 3, *P < 0.05). (**G**) Effect of autophagy on HYF127c/Cu-induced oxidative stress indicated by DCF. (i) FACS results of HYF127c/Cu-treated *Atg7*$^{+/+}$ MEFs. (ii) FACS results of HYF127c/Cu-treated *atg7*$^{-/-}$ MEFs. (iii) FACS results of HeLa cells treated with both HYF127c/Cu and CQ. (iv) FACS results of HeLa cells treated with both HYF127c/Cu and 3-MA. (v) FACS results of HeLa cells treated with both HYF127c/Cu and rapamycin.

Above all, our results showed that the MAPK11/12/13/14 pathway was activated in HYF127c/Cu-treated HeLa cells. It has been reported that physalin A can induce ROS-mediated apoptosis, and autophagy plays a protective role through the MAPK11/12/13/14-NFKB/NF-kappaB survival pathway.[45] Another finding suggests that the MAPK11/12/13/14 pathway participates in mediating oxidative stress-induced autophagy-related genes such as *ATG7*.[46] Our results showed that activation of the MAPK11/12/13/14 pathway is responsible for significant upregulation of autophagy genes (e.g., *BAG3*, *MAP1LC3B*, and *HSPA1A*), which contributes to the increase of autophagy. These results indicate that the MAPK11/12/13/14 pathway participates in the transcriptional regulation of protective autophagy in response to oxidative stress.

In conclusion, our results show that a novel copper complex HYF127c/Cu efficiently induces cancer cell death though copper-dependent oxidative stress. Transcriptional analysis by RNA-Seq reveals that the copper complex can modulate multiple signal pathways in cancer cells, in which protective autophagy is activated through MAPK11/12/13/14-mediated transcriptional upregulation of autophagy genes.

Materials and Methods

Synthesis of HYF127c

Figure 11 shows the synthesis of intermediates of 4-allyl-3-selenosemicarbazide.

1.32 g (10 mmol) 4-Ally-3-thiosemicarbazide (Matrix, 056882) was dissolved in about 10 ml ethanol, and 1.42 g (10 mmol) methyl iodide (SCRC, 80084117) was added. The mixture was heated on reflux for 1 h. This afforded the ethanolic solution of s-methy-4-allythiosemicarbazide.

A 50-ml dry 3-necked-bottle was placed in an ice-bath. 0.95 g (12 mmol) Se and 0.57 g (15 mmol) NaBH4 (SCRC, 80115860) were added under nitrogen atmosphere and were heated up before adding 10 ml ethanol. 0.64 g (6 mmol) Na_2CO_3 was added after 1 h. Then the ice-bath was removed and the ethanolic solution of s-methy-4-Allythiosemicarbazide was added. The reaction continued for 20 h at room temperature, then 1 ml acetic acid was added and absorbed with an exhaust by an acetic acid lead solution (10%, 200 ml) by dissolving 20 g acetic acid lead (SCRC,10012418) in 200 ml water. The reaction solution was filtered. The solvent was evaporated under reduced pressure. The residue was purified by column chromatography on silica gel (Haiyang, 20034365) of EA-PE (1:1, v/v); yield 0.90 g (51%). ^{1}H-NMR (400 MHz, DMSO) δppm:4.139 (m, ^{2}H) 4.529 (m, ^{2}H) 5.074~5.142 (m, ^{2}H) 5.829~5.872 (m, ^{1}H) 8.208 (m, ^{1}H) 9.150 (m, ^{1}H).

The synthesis of di-2-pyridyl ketone 4-allyl-3-selenosemicarbazide

Di-2-pyridyl ketone (0.368 g, 2 mmol) was dissolved in ethanol (EtOH; 5 ml 99% EtOH). A solution of 4-allyl-3-selenosemicarbazide in EtOH was added followed by glacial acetic acid (1 ml) and the mixture was refluxed for 4 h. The yellow precipitate was collected by vacuum filtration and recrystalized from ethyl acetate; yield (0.33 g, 49%). 1H-NMR (400 MHz, DMSO) δppm: 4.3296~4.3584 (m, ^{2}H) 5.1507~5.2222 (m, ^{2}H) 5.8968~5.9396 (m, ^{1}H) 7.4949~7.5299 (m, ^{2}H) 7.6112 (m, ^{1}H) 7.9706~8.0056 (m, ^{2}H) 8.2648~8.2844 (d, ^{1}H) 8.5801~8.5920 (d, ^{1}H) 8.8295~8.8421 (d, ^{1}H) 9.4460~9.4754 (m, ^{1}H) 13.5766 (s, ^{1}H) HLPC-MS m/z:346.2 [M+1]+.

Chemicals and antibodies

Chemicals and antibodies were purchased as follows: H_2DCF (Beyotime, S0033), N-acety-L-cysteine (Sigma, A7250), 3-methyladenine (Sigma, M9281), propidium iodide (Sigma, P4170), chloroquine diphosphate (Sigma, C6628), Necrostatin-1 (Sigma, N9037), rapamycin (Sigma, R0395), SB203580 (Sigma, S8037), SP100625 (Sigma, S5567), Lipofectamine 2000 (Invitrogen, 11668-019), rabbit anti-LC3 (Cell Signaling, 3868S), rabbit anti-ATG7 (Sigma, A2856), rabbit anti-MAPK14/p38α (Bioworld, BS3566), rabbit anti-p-MAPK11/12/13/14 (Santa Cruz, sc-17852R), rabbit anti-p-MAPKAPK2/MK2 (Cell Signaling, 3316P), rabbit anti-PARP1 (Cell Signaling, 9542P), rabbit anti-CASP3 (Cell Signaling, 9662s), rabbit anti-GAPDH (Earthox, E021060), rabbit anti-SQSTM1 (MBL, PM045), mouse anti-ACTB (Bioworld, BSAP500060), goat anti-mouse IgG (Bioworld, BS13278), goat anti-rabbit IgG (Bioworld, BS12478), ANXA5-EGFP Apoptosis Detection Kit (Vigorous, A002), copper (II) chloride ($CuCl_2$, Beijing Shiji, China). HYF127c/Cu was freshly prepared by mixing equal volumes of 100 mmol HYF127c and 100 mmol $CuCl_2$, then diluted to the appropriate concentrations before treatment.

Cell culture

HeLa, MCF-7, and H1299 cell lines were obtained from The Cell Bank of the Chinese Academy of Sciences (Shanghai), cells were cultured in Dulbecco's modified Eagle's medium (HyClone, SH30022.01B) supplemented with 10% fetal bovine serum at 37 °C in an atmosphere of 5% CO_2. Atg7-deficient (*atg7*$^{-/-}$) MEF

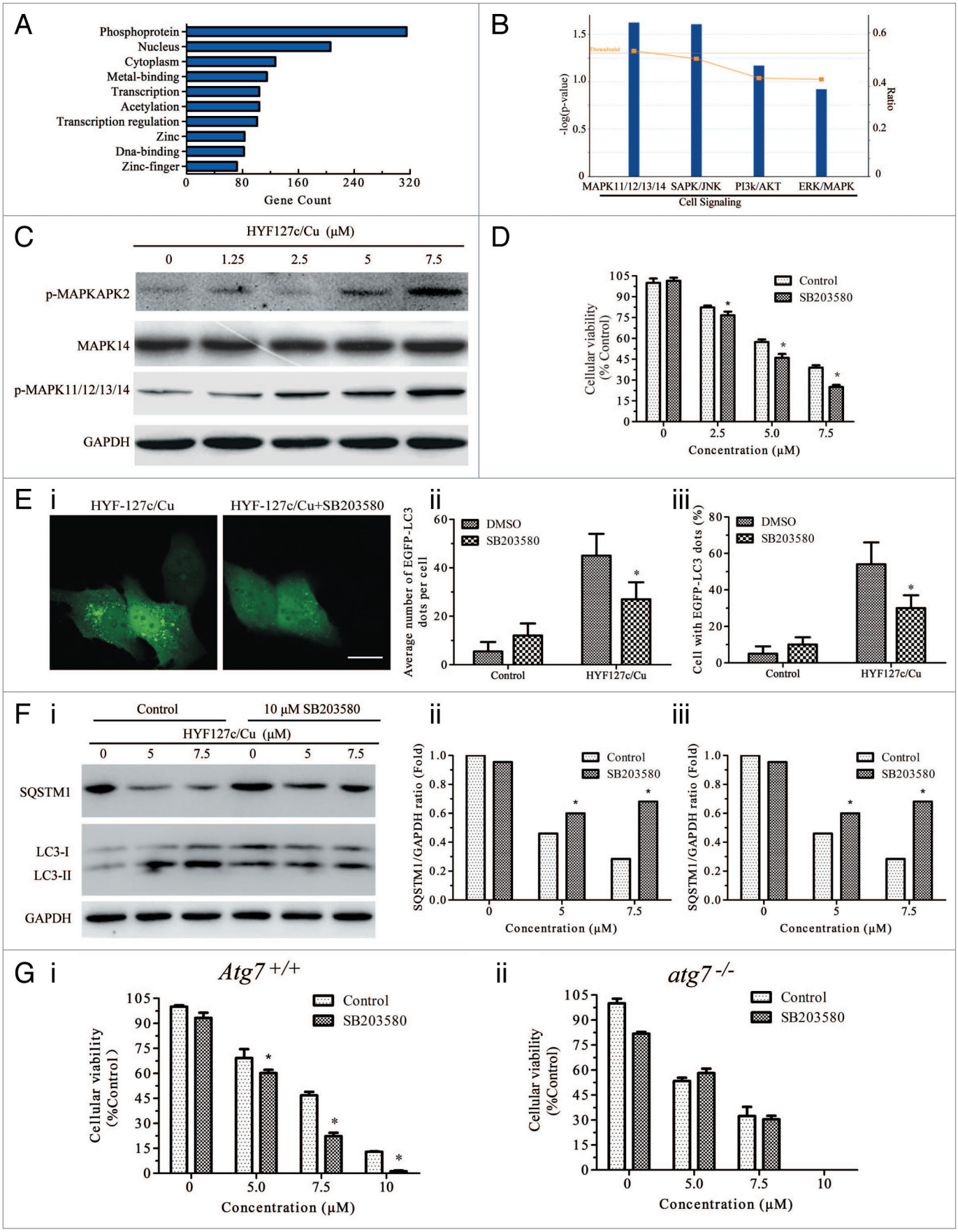

Figure 9. For figure legend, see page 1297.

Figure 9 (See opposite page). The MAPK11/12/13/14 (p38 MAPK) inhibitor SB203580 decreases HYF127c/Cu-induced autophagy. (**A**) The function of 652 genes (fold > 1 or fold < −1, $P < 0.01$) analyzed by DAVID. (**B**) IPA analysis of phosphorylation pathways possibly involved in HYF127c/Cu-induced autophagy and cell death. (**C**) Phosphorylation of MAPK11/12/13/14 (p38 MAPK) and its downstream target protein MAPKAPK2 in HYF127c/Cu-treated HeLa cells. (**D**) Effect of the combination of SB203580 and HYF127c/Cu on cellular viability in HeLa cells, (n = 3, *$P < 0.05$). (**E**) Decreased punctate distribution of EGFP-LC3 in cells treated with HYF127c/Cu and SB203580 (i). Bar, 20 μM. The percentage of cells with evident accumulation of EGFP-LC3 dots (ii) and the average number of EGFP-LC3 dots in cells (iii) (n = 3, *$P < 0.05$). (**F**) Western blot results of SQSTM1 and LC3 in cells treated with both HYF127c/Cu and SB203580 or treated with HYF127c/Cu alone. (**G**) The effect of SB203580 on cellular viability of HYF127c/Cu-treated *Atg7*$^{+/+}$ and *atg7*$^{-/-}$ cells (n = 3, *$P < 0.05$).

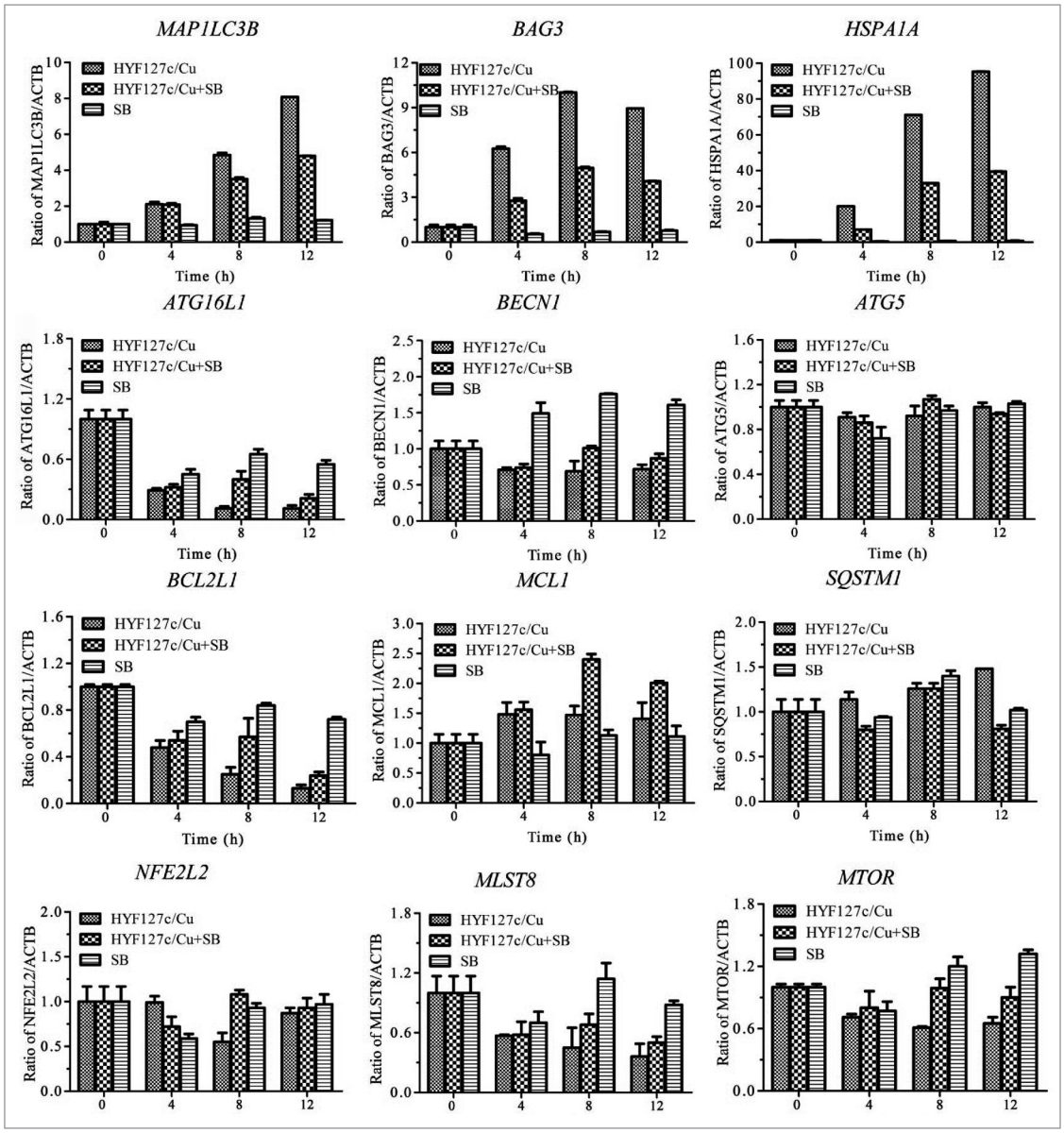

Figure 10. Analysis of the MAPK11/12/13/14 (p38 MAPK) inhibitor SB203580 on transcription. The effect of SB203580 on the transcription of *BAG3*, *MAP1LC3B*, *HSPA1A* and other genes (*SQSTM1*, *ATG16L1*, *BECN1*, *ATG5*, *MTOR*, *BCL2L1*, *MCL1*, *NEFL2*, and *MLST8*) at different time points (0, 4, 8 and 12 h) (n = 3, *$P < 0.05$).

cells and control (*Atg7*$^{+/+}$) MEF cells were generous gifts from Dr Yingyu Chen and were cultured in Dulbecco's modified Eagle's medium supplemented with 10% fetal bovine serum and 200 μg/ml amphotericin. Cell lines were authenticated based on viability, recovery, growth, morphology, and also cytogenetic analysis, antigen expression, DNA profile, and isoenzymology by the provider.

Cell viability

Cell viability was measured by using 3-(4,5)-dimethylthiahiazo (-z-y1)-3,5-di-phenytetrazoliumromide (MTT) assay (Sigma,

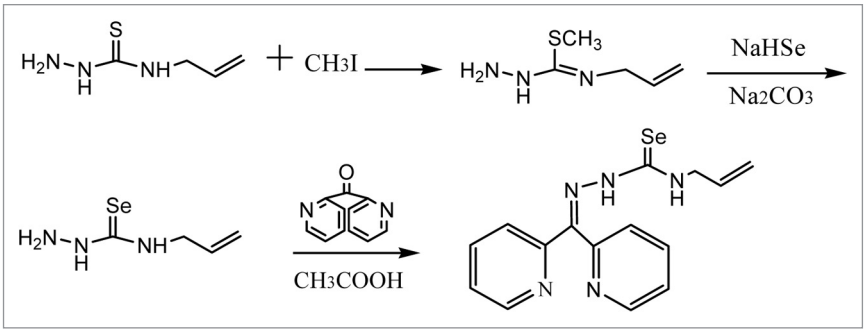

Figure 11. The synthesis of intermediates of 4-allyl-3-selenosemicarbazide.

M5655). About 3000 cells were plated in each well of 96-well plates at 37 °C in a humidified 5% CO_2 for 12 h before being treated with the indicated compounds. After treatment, 20 μl MTT (5 mg/ml) solution was added to each well, and the cultures incubated for 4 h at 37 °C in humidified 5% CO_2. The medium was extracted to stop the reaction, then 150 μl dimethylsulfoxide (DMSO) was added and measured with a Varioskan Flash reader (Thermofisher, varioskan Flash, USA) at 490 nm. Each sample was repeated 3 times for standard deviation calculations.

Analysis of oxidative stress

The intracellular accumulation of oxidative stress was detected using a H_2DCF probe. Ten micrometers H_2DCF was added into HYF127c/Cu-treated or control cells for 30 min, then cells were harvested and analyzed with a FACSCalibur (Becton Dickinson, USA).

GSH/GSSG assay

GSH/GSSG assay was measured with a kit (Beyotime, S0053). HeLa cells were treated with DMSO, Cu, HYF127c, HYF127c/Cu, and H_2O_2 for 12 h at 37 °C in an atmosphere of 5% CO_2.

RNA-Seq

Total RNA was extracted from HYF127c/Cu-treated cells and control cells using the RNeasy Mini Kit (Qiagen, 74104) according to the manufacturer's protocol, and then treated with DNase I (Qiagen, 79254) for 15 min at room temperature to remove residual genomic DNA. The purity of RNA extraction was assayed with a NanoDrop 2000 (Thermofisher, ND-2000C, USA), the 260/280 ratio needed to be between 1.8 and 2.0 and RNA was checked by running a sample of fragmented RNA on a RNA Pico 6000 chip in an Agilent 2100 Bioanalyzer (Agilent Technologies, Agilent 2100, USA). Briefly, total RNA (1 μg) was used to isolate mRNAs with poly(A) tails and then these mRNAs were converted to cDNA using the TruSeq DNA Sample Preparation Kit (Illumina, FC-121-2001) according to the manufacturer's protocol. After generation of the target cDNA from HeLa cells, sequencing adapters were ligated to short fragments after purification with a QiaQuick PCR extraction kit (QIAGEN, 28104), and were used to examine different sequences in the samples. Fragments with lengths ranging from 200 to 700 bp were then separated by agarose gel electrophoresis and the fragments were subjected to 15 cycles of PCR amplification. Finally, the prepared libraries were sequenced using an Illumina HiSeq™ 2000 system (Illumina, USA) before being assessed by q-PCR with an Agilent 2100 Bioanalyzer. The results obtained from each cell were matched to the human genome (NCBI Build 36); results that aligned with specificity were used in the downstream analysis. Unambiguously mapped results were first used to generate gene counts. Feature counts were normalized using the RPKM (read per kilobases per million aligned reads) method. The RPKM method is able to eliminate the influence of different gene length and sequencing discrepancy on the calculation of gene expression. Therefore, the calculated gene expression can be directly used for comparing the difference of gene expression among samples. To detect different expression levels among different stages, the *P* value (1-tailed) corresponds to the differential gene expression test (2-sample *t* test with equal variances) Since differentially expressed gene analysis generates large multiplicity problems in which thousands of hypotheses (i.e., whether a particular gene is differentially expressed between the 2 groups) are tested simultaneously. Corrections for false positive (type I errors) and false negative (type II) errors were performed using the false discovery rate (FDR) method.

Transient transfection and confocal microscopy

About 1.4×10^5 cells were plated into each well of a 24-well plate 24 h before transfection. Plasmids (800 ng/well) or siRNA (660 ng/well) were transfected with Lipofectamine 2000 according to the manufacturer's protocol. Both fixed and live cells were imaged by using an A1R-si Laser Scanning Confocal Microscope (Nikon, Japan). To measure the formation of autophagosomes, HeLa cells were transfected with plasmids encoding EGFP-LC3. The accumulation and distribution of EGFP-LC3 puncta were recorded using an A1R-si Laser Scanning Confocal Microscope. Ten fields of cells with EGFP-LC3 puncta were counted. The number of EGFP-LC3 puncta per cell was counted for 50 cells.

Western blot analysis

To analyze protein expression, western blotting was performed as described previously.[33,39]

Transmission electron microscopy

Transmission electron microscopy was performed following previously described methods.[33,39]

Real-time PCR

RNA isolation was performed from HeLa cells harvested after different times following treatment. cDNA was synthesized using 2 μg of total RNA by High Capacity RNA-to-cDNA kit (Applied Biosystems, 4387406) following the protocol provided. Fifty nanograms cDNA was used for qRT-PCR. One micrometer of cDNA was used and primers (**Table S2**) were added to the PCR reaction at a concentration of 300 nM. All other components from the PCR reaction were from the SYBR Premix Ex Taq™ II Kit (TaKaRa, DRR820A). The PCR cycling was performed with an ABI 7500 system (Applied Biosystems, USA) followed by melting-curve analysis. The relative differences in RNA expression in samples with different treatments and exposure times were assessed by the comparative Ct method using threshold cycle (Ct) values. Briefly, Ct values were first normalized to that of *ACTB*/β-actin in the same sample (dCt) and then differences of Ct values between each treated and control group (ddCt) were used to calculate the changes of fold-induction in each sample using the formula 2^{ddCt}. All qPCR experiments were done for 2 donors in triplicate by using three different reverse transcription reactions of RNA samples, and the results were averaged.

Xenograft study

The 6-wk-old female nude mice (BALB/c-nu) were purchased from the Vital River Laboratories (China) and fed in the laboratory animal center of Peking University (AAALACi-accredited facility). HeLa cells were injected subcutaneously into the flanks of the mice (5×10^6 in 200 μL). After injection,tumors were allowed to develop for 15 d until they reached 100 mm^3. Then 30 mice were allocated into 3 groups of 10 mice per group. The 3 groups respectively included DMSO in 0.9% saline (control), 10 mg/kg HYF127c and 10 mg/kg HYF127c·Cu. The mice in the 3 groups were i.g. (intragastric administration) injected daily according to their weight. The tumor size was measured using calipers, and tumor volume was estimated according to the following formula: tumor volume (mm^3) = L × W2/ 2, where L is the length and W is the width. Tumor-bearing mice were sacrificed after 15 d. Xenograft tumors were harvested to be weighed and fixed in 4% formalin for histological study.

Histopathological study

Tissues were harvested and fixed in 10% buffered formalin. The histological examination used standard techniques. Then, kidney, myocardium, and liver were embedded in paraffin, sectioned, and stained by hematoxylin and eosin. After hematoxylin and eosin staining, the slides were examined and photos were taken with an optical microscope (Nikon, Japan).

Statistical analysis

Each experiment was repeated at least 3 times for standard deviation calculations. The statistical significance of differences was assessed using the Student *t* test in GraphPad prism 5. A *P* value less than 0.05 considered statistically significant.

Disclosure of Potential Conflicts of Interest

No potential conflicts of interest were disclosed.

Acknowledgments

This work was supported by grant No. 2011CB910103 to Jian Lin from the 973 Program, and grant No. 31071209 to Jian Lin from the National Science Foundation of China, and grant No. 2011BAI18B01 to Wu Zhong from the National Key Technology R&D Program.

Supplemental Materials

Supplemental materials may be found here:
www.landesbioscience.com/journals/autophagy/article/28789

Reference

1. Skrott Z, Cvek B. Diethyldithiocarbamate complex with copper: the mechanism of action in cancer cells. Mini Rev Med Chem 2012; 12:1184-92; PMID:22931589; http://dx.doi.org/10.2174/138955712802762068
2. Loganathan R, Ramakrishnan S, Suresh E, Riyasdeen A, Akbarsha MA, Palaniandavar M. Mixed ligand copper(II) complexes of N,N-bis(benzimidazol-2-ylmethyl)amine (BBA) with diimine co-ligands: efficient chemical nuclease and protease activities and cytotoxicity. Inorg Chem 2012; 51:5512-32; PMID:22559171; http://dx.doi.org/10.1021/ic2017177
3. Gandin V, Pellei M, Tisato F, Porchia M, Santini C, Marzano C. A novel copper complex induces paraptosis in colon cancer cells via the activation of ER stress signalling. J Cell Mol Med 2012; 16:142-51; PMID:21388518; http://dx.doi.org/10.1111/j.1582-4934.2011.01292.x
4. Duff B, Thangella VR, Creaven BS, Walsh M, Egan DA. Anti-cancer activity and mutagenic potential of novel copper(II) quinolinone Schiff base complexes in hepatocarcinoma cells. Eur J Pharmacol 2012; 689:45-55; PMID:22705894; http://dx.doi.org/10.1016/j.ejphar.2012.06.004
5. Frezza M, Hindo S, Chen D, Davenport A, Schmitt S, Tomco D, Dou QP. Novel metals and metal complexes as platforms for cancer therapy. Curr Pharm Des 2010; 16:1813-25; PMID:20337575; http://dx.doi.org/10.2174/138161210791209009
6. Chen D, Dou QP. New uses for old copper-binding drugs: converting the pro-angiogenic copper to a specific cancer cell death inducer. Expert Opin Ther Targets 2008; 12:739-48; PMID:18479220; http://dx.doi.org/10.1517/14728222.12.6.739
7. Chen D, Milacic V, Frezza M, Dou QP. Metal complexes, their cellular targets and potential for cancer therapy. Curr Pharm Des 2009; 15:777-91; PMID:19275642; http://dx.doi.org/10.2174/138161209787582183
8. Kelland L. The resurgence of platinum-based cancer chemotherapy. Nat Rev Cancer 2007; 7:573-84; PMID:17625587; http://dx.doi.org/10.1038/nrc2167
9. Tardito S, Marchiò L. Copper compounds in anticancer strategies. Curr Med Chem 2009; 16:1325-48; PMID:19355889; http://dx.doi.org/10.2174/092986709787846532
10. Jungwirth U, Kowol CR, Keppler BK, Hartinger CG, Berger W, Heffeter P. Anticancer activity of metal complexes: involvement of redox processes. Antioxid Redox Signal 2011; 15:1085-127; PMID:21275772; http://dx.doi.org/10.1089/ars.2010.3663
11. Duncan C, White AR. Copper complexes as therapeutic agents. Metallomics 2012; 4:127-38; PMID:22187112; http://dx.doi.org/10.1039/c2mt00174h
12. Chen D, Cui QC, Yang H, Dou QP. Disulfiram, a clinically used anti-alcoholism drug and copper-binding agent, induces apoptotic cell death in breast cancer cultures and xenografts via inhibition of the proteasome activity. Cancer Res 2006; 66:10425-33; PMID:17079463; http://dx.doi.org/10.1158/0008-5472.CAN-06-2126
13. Lovejoy DB, Jansson PJ, Brunk UT, Wong J, Ponka P, Richardson DR. Antitumor activity of metal-chelating compound Dp44mT is mediated by formation of a redox-active copper complex that accumulates in lysosomes. Cancer Res 2011; 71:5871-80; PMID:21750178; http://dx.doi.org/10.1158/0008-5472.CAN-11-1218
14. Tardito S, Bassanetti I, Bignardi C, Elviri L, Tegoni M, Mucchino C, Bussolati O, Franchi-Gazzola R, Marchiò L. Copper binding agents acting as copper ionophores lead to caspase inhibition and paraptotic cell death in human cancer cells. J Am Chem Soc 2011; 133:6235-42; PMID:21452832; http://dx.doi.org/10.1021/ja109413c
15. Klionsky DJ, Abdalla FC, Abeliovich H, Abraham RT, Acevedo-Arozena A, Adeli K, Agholme L, Agnello M, Agostinis P, Aguirre-Ghiso JA, et al. Guidelines for the use and interpretation of assays for monitoring autophagy. Autophagy 2012; 8:445-544; PMID:22966490; http://dx.doi.org/10.4161/auto.19496

16. Sun Y, Zou M, Hu C, Qin Y, Song X, Lu N, et al. Wogonoside induces autophagy in MDA-MB-231 cells by regulating MAPK-mTOR pathway. Food and chemical toxicology: an international journal published for the British Industrial Biological Research Association 2013; 51:53-60.
17. Zhou Z, Zhang D, Yang L, Ma P, Si Y, Kortz U, Niu J, Wang J. Nona-copper(II)-containing 18-tungsto-8-arsenate(III) exhibits antitumor activity. Chem Commun (Camb) 2013; 49:5189-91; PMID:23628910; http://dx.doi.org/10.1039/c3cc41628c
18. Trejo-Solís C, Jimenez-Farfan D, Rodriguez-Enriquez S, Fernandez-Valverde F, Cruz-Salgado A, Ruiz-Azuara L, Sotelo J. Copper compound induces autophagy and apoptosis of glioma cells by reactive oxygen species and JNK activation. BMC Cancer 2012; 12:156; PMID:22540380; http://dx.doi.org/10.1186/1471-2407-12-156
19. Sun T, Yan Y, Zhao Y, Guo F, Jiang C. Copper oxide nanoparticles induce autophagic cell death in A549 cells. PLoS One 2012; 7:e43442; PMID:22916263; http://dx.doi.org/10.1371/journal.pone.0043442
20. Hancock CN, Stockwin LH, Han B, Divelbiss RD, Jun JH, Malhotra SV, Hollingshead MG, Newton DL. A copper chelate of thiosemicarbazone NSC 689534 induces oxidative/ER stress and inhibits tumor growth in vitro and in vivo. Free Radic Biol Med 2011; 50:110-21; PMID:20971185; http://dx.doi.org/10.1016/j.freeradbiomed.2010.10.696
21. Guo WJ, Ye SS, Cao N, Huang J, Gao J, Chen QY. ROS-mediated autophagy was involved in cancer cell death induced by novel copper(II) complex. Experimental and toxicologic pathology: official journal of the Gesellschaft fur Toxikologische Pathologie 2010; 62:577-82.
22. Paris I, Perez-Pastene C, Couve E, Caviedes P, Ledoux S, Segura-Aguilar J. Copper dopamine complex induces mitochondrial autophagy preceding caspase-independent apoptotic cell death. J Biol Chem 2009; 284:13306-15; PMID:19265190; http://dx.doi.org/10.1074/jbc.M900323200
23. Myhre O, Andersen JM, Aarnes H, Fonnum F. Evaluation of the probes 2′,7′-dichlorofluorescin diacetate, luminol, and lucigenin as indicators of reactive species formation. Biochem Pharmacol 2003; 65:1575-82; PMID:12754093; http://dx.doi.org/10.1016/S0006-2952(03)00083-2
24. Meister A, Anderson ME. Glutathione. Annu Rev Biochem 1983; 52:711-60; PMID:6137189; http://dx.doi.org/10.1146/annurev.bi.52.070183.003431
25. Wang Z, Gerstein M, Snyder M. RNA-Seq: a revolutionary tool for transcriptomics. Nat Rev Genet 2009; 10:57-63; PMID:19015660; http://dx.doi.org/10.1038/nrg2484
26. Ozsolak F, Milos PM. RNA sequencing: advances, challenges and opportunities. Nat Rev Genet 2011; 12:87-98; PMID:21191423; http://dx.doi.org/10.1038/nrg2934
27. Wacker SA, Houghtaling BR, Elemento O, Kapoor TM. Using transcriptome sequencing to identify mechanisms of drug action and resistance. Nat Chem Biol 2012; 8:235-7; PMID:22327403; http://dx.doi.org/10.1038/nchembio.779
28. Rouschop KM, van den Beucken T, Dubois L, Niessen H, Bussink J, Savelkouls K, Keulers T, Mujcic H, Landuyt W, Voncken JW, et al. The unfolded protein response protects human tumor cells during hypoxia through regulation of the autophagy genes MAP1LC3B and ATG5. J Clin Invest 2010; 120:127-41; PMID:20038797; http://dx.doi.org/10.1172/JCI40027
29. Zhang XY, Wu XQ, Deng R, Sun T, Feng GK, Zhu XF. Upregulation of sestrin 2 expression via JNK pathway activation contributes to autophagy induction in cancer cells. Cell Signal 2013; 25:150-8; PMID:22982090; http://dx.doi.org/10.1016/j.cellsig.2012.09.004
30. Carra S, Seguin SJ, Landry J. HspB8 and Bag3: a new chaperone complex targeting misfolded proteins to macroautophagy. Autophagy 2008; 4:237-9; PMID:18094623
31. Behl C. BAG3 and friends: co-chaperones in selective autophagy during aging and disease. Autophagy 2011; 7:795-8; PMID:21681022; http://dx.doi.org/10.4161/auto.7.7.15844
32. Yang Y, Fiskus W, Yong B, Atadja P, Takahashi Y, Pandita TK, Wang HG, Bhalla KN. Acetylated hsp70 and KAP1-mediated Vps34 SUMOylation is required for autophagosome creation in autophagy. Proc Natl Acad Sci U S A 2013; 110:6841-6; PMID:23569248; http://dx.doi.org/10.1073/pnas.1217692110
33. Lin J, Zheng Z, Li Y, Yu W, Zhong W, Tian S, Zhao F, Ren X, Xiao J, Wang N, et al. A novel Bcl-XL inhibitor Z36 that induces autophagic cell death in Hela cells. Autophagy 2009; 5:314-20; PMID:19242113; http://dx.doi.org/10.4161/auto.5.3.7888
34. Malik SA, Shen S, Mariño G, BenYounès A, Maiuri MC, Kroemer G. BH3 mimetics reveal the network properties of autophagy-regulatory signaling cascades. Autophagy 2011; 7:914-6; PMID:21508685; http://dx.doi.org/10.4161/auto.7.8.15785
35. Zhou F, Yang Y, Xing D. Bcl-2 and Bcl-xL play important roles in the crosstalk between autophagy and apoptosis. FEBS J 2011; 278:403-13; PMID:21182587; http://dx.doi.org/10.1111/j.1742-4658.2010.07965.x
36. Klionsky DJ, Abeliovich H, Agostinis P, Agrawal DK, Aliev G, Askew DS, Baba M, Baehrecke EH, Bahr BA, Ballabio A, et al. Guidelines for the use and interpretation of assays for monitoring autophagy in higher eukaryotes. Autophagy 2008; 4:151-75; PMID:18188003
37. Hanahan D, Weinberg RA. Hallmarks of cancer: the next generation. Cell 2011; 144:646-74; PMID:21376230; http://dx.doi.org/10.1016/j.cell.2011.02.013
38. Kondo Y, Kanzawa T, Sawaya R, Kondo S. The role of autophagy in cancer development and response to therapy. Nat Rev Cancer 2005; 5:726-34; PMID:16148885; http://dx.doi.org/10.1038/nrc1692
39. Tian S, Lin J, Jun Zhou J, Wang X, Li Y, Ren X, Yu W, Zhong W, Xiao J, Sheng F, et al. Beclin 1-independent autophagy induced by a Bcl-XL/Bcl-2 targeting compound, Z18. Autophagy 2010; 6:1032-41; PMID:20818185; http://dx.doi.org/10.4161/auto.6.8.13336
40. Whitmarsh AJ. A central role for p38 MAPK in the early transcriptional response to stress. BMC Biol 2010; 8:47; PMID:20515460; http://dx.doi.org/10.1186/1741-7007-8-47
41. Bazuine M, Carlotti F, Rabelink MJ, Vellinga J, Hoeben RC, Maassen JA. The p38 mitogen-activated protein kinase inhibitor SB203580 reduces glucose turnover by the glucose transporter-4 of 3T3-L1 adipocytes in the insulin-stimulated state. Endocrinology 2005; 146:1818-24; PMID:15665038; http://dx.doi.org/10.1210/en.2004-1347
42. Bennett BL, Sasaki DT, Murray BW, O'Leary EC, Sakata ST, Xu W, Leisten JC, Motiwala A, Pierce S, Satoh Y, et al. SP600125, an anthrapyrazolone inhibitor of Jun N-terminal kinase. Proc Natl Acad Sci U S A 2001; 98:13681-6; PMID:11717429; http://dx.doi.org/10.1073/pnas.251194298
43. Hancock CN, Stockwin LH, Han B, Divelbiss RD, Jun JH, Malhotra SV, Hollingshead MG, Newton DL. A copper chelate of thiosemicarbazone NSC 689534 induces oxidative/ER stress and inhibits tumor growth in vitro and in vivo. Free Radic Biol Med 2011; 50:110-21; PMID:20971185; http://dx.doi.org/10.1016/j.freeradbiomed.2010.10.696
44. White E. Deconvoluting the context-dependent role for autophagy in cancer. Nat Rev Cancer 2012; 12:401-10; PMID:22534666; http://dx.doi.org/10.1038/nrc3262
45. He H, Zang LH, Feng YS, Chen LX, Kang N, Tashiro S, Onodera S, Qiu F, Ikejima T. Physalin A induces apoptosis via p53-Noxa-mediated ROS generation, and autophagy plays a protective role against apoptosis through p38-NF-κB survival pathway in A375-S2 cells. J Ethnopharmacol 2013; 148:544-55; PMID:23684722; http://dx.doi.org/10.1016/j.jep.2013.04.051
46. McClung JM, Judge AR, Powers SK, Yan Z. p38 MAPK links oxidative stress to autophagy-related gene expression in cachectic muscle wasting. Am J Physiol Cell Physiol 2010; 298:C542-9; PMID:19955483; http://dx.doi.org/10.1152/ajpcell.00192.2009